

1 **DNA origami-based single-molecule force spectroscopy unravels the**
2 **molecular basis of RNA Polymerase III pre-initiation complex stability**

3

4 Kevin Kramm¹, Tim Schröder², Jerome Gouge³, Andrés Manuel Vera², Florian B. Heiss⁴,
5 Tim Liedl⁵, Christoph Engel⁴, Alessandro Vannini^{3,6}, Philip Tinnefeld² and Dina
6 Grohmann^{1,4}

7

8 ¹ Institute of Microbiology & Archaea Centre, Single-Molecule Biochemistry Lab,
9 University of Regensburg, 93053 Regensburg, Germany

10 ² Department of Chemistry and Center for NanoScience (CeNS), Ludwig-Maximilians-
11 Universität München, 80539 München, Germany

12 ³ The Institute of Cancer Research, London SW7 3RP, UK

13 ⁴ Biochemistry Centre Regensburg, University of Regensburg, 93053 Regensburg,
14 Germany

15 ⁵ Faculty of Physics and Center for Nanoscience (CeNS), Ludwig-Maximilians-Universität
16 München, 80539 Munich, Germany

17 ⁶ Human Technopole Foundation, Centre of Structural Biology, 20157 Milan, Italy

18

19

20 *For correspondence:

21 Dina Grohmann, Department of Biochemistry, Genetics and Microbiology, Institute of
22 Microbiology, University of Regensburg, Universitätsstraße 31, 93053 Regensburg,
23 Germany

24 e-mail: dina.grohmann@ur.de

25 Tel.: 0049 941 943 3147

26 Fax: 0049 941 943 2403

27

28 **Keywords:** DNA origami, TBP, TFIIB, Bdp1, transcription, single-molecule FRET, single-
29 molecule force measurements, RNA polymerase

30

31 **Abstract**

32 The TATA-binding protein (TBP) and a transcription factor (TF) IIB-like factor compound
33 the fundamental core of all eukaryotic initiation complexes. The reason for the
34 emergence and strict requirement of the additional initiation factor Bdp1, which is
35 unique to the RNA polymerase (RNAP) III system, however, remained elusive. A poorly
36 studied aspect in this context is the effect of DNA strain, that arises from DNA
37 compaction and transcriptional activity, on the efficiency of initiation complex
38 formation. We made use of a new nanotechnological tool – a DNA origami-based force
39 clamp - to follow the assembly of human initiation complexes in the Pol II and Pol III
40 system at the single-molecule level under piconewton forces. We demonstrate that
41 TBP-DNA complexes are force-sensitive and TFIIB is necessary and sufficient to stabilise
42 TBP on a strained RNAP II promoter. In contrast, Bdp1 is the pivotal component that
43 ensures stable anchoring of initiation factors, and thus the polymerase itself, in the
44 RNAP III system. Thereby, we offer an explanation for the crucial role of Bdp1 for the
45 high transcriptional output of Pol III genes for the first time.

46

47

48

49 Introduction

50 All cellular life depends on the regulated expression of its genome. The first step in
51 gene expression is transcription, which is carried out by highly conserved multisubunit
52 RNA polymerases (RNAP) that make use of a DNA template to synthesise RNA¹.
53 Transcription is a cyclic process that can be divided into the initiation, elongation and
54 termination phase. Aided by a number of basal transcription initiation factors, the
55 archaeal-eukaryotic RNAP is recruited to the promoter DNA thereby positioning the
56 RNAP at the transcription start site (TSS)²⁻³. All archaeal-eukaryotic RNAPs rely on the
57 basal transcription initiation factor TBP and a TFIIB-like factor^{4,5 6,7}, despite some
58 particularities of the Pol I system⁸. TBP is highly conserved in structure and function
59 and recognises an AT-rich DNA stretch, the so-called TATA-box (eukaryotic consensus
60 sequence TATAWAWR with W = T or A and R = G or A⁹), upstream of the TSS¹⁰⁻¹⁴.
61 Canonical binding of TBP to the DNA invokes a 90° bend in the DNA¹⁵⁻¹⁷ when two
62 conserved pairs of phenylalanines are inserted into the promoter DNA between bases
63 1/2 and 7/8 of the TATA box sequence. Bending leads to a widening of the minor groove
64 of the promoter DNA¹⁶. TFIIB-like factors associate with the TBP-DNA complex via the
65 C-terminal core domain and concomitantly recognise the B-recognition element (BRE)
66 located adjacent to the TATA-box^{8,18-23}. Even though additional factors (e.g. TFIIE,
67 TFIIH, TFIIIF) are involved in the initiation process *in vivo*²⁴, the minimal configuration
68 of TBP and TFIIB factor are sufficient to to recruit the RNAP (in complex with TFIIIF) to
69 the promoter in eukaryotic RNAP II transcription system²⁵⁻²⁹. While the eukaryotic
70 RNAP II system is responsible for the transcription of messenger RNAs and small
71 nucleolar (sn)RNAs, RNAP transcription systems I and III are transcribing ribosomal (r)
72 RNAs and 5S rRNA, U6 snRNA, tRNAs, respectively. The initiation factor setup in the
73 specialised RNAP I and III transcriptions systems, however, diverged from the
74 composition of the RNAP II system and additional initiation factors are required for
75 efficient initiation^{7,8,30}. While TBP was found to be part of the RNAP I initiation
76 machinery *in vivo*³¹⁻³³, basal transcriptional activity can also be achieved in the absence
77 of TBP³⁴⁻³⁶ and its functional role in the RNAP I system remains elusive. RNAP III
78 transcription is directed from three different promoter classes that differ in promoter
79 elements and initiation factor requirement^{6,37}. In all cases, transcription initiation in

80 the RNAP III system relies on the multisubunit factor TFIIIB composed of TBP, the TFIIIB-
81 like factors Brf1 and Bdp1 (B double prime or B'')^{7,21}. Bdp1 is unique to RNAP III
82 transcription initiation and has no homologue in the RNAP I or II transcription system.
83 However, Bdp1 is crucially involved in promoter recognition and DNA opening^{38,39}.
84 Vertebrates additionally use a TFIIIB variant that contains Brf2 instead of Brf1. Both
85 factors are structurally similar, but Brf2 binding to the TBP-DNA complex is regulated
86 by the redox state of the cell. The Brf2 containing TFIIIB complex initiates transcription
87 at a small subset of genes, including the selenocysteine tRNA and U6 snRNA. In contrast
88 to Pol II- transcribed snRNA genes, the U6 promoter contains a TATA-box element that
89 is crucial for the specific recruitment of TFIIIB^{38,40,41}. TFIIIB is sufficient for the
90 recruitment of yeast RNAP III *in vitro*⁴². However, at human type 3 promoters an
91 additional protein complex is involved in transcription initiation, the snRNA activating
92 protein complex (SNAP_c, reviewed in³⁷).

93 In addition to biochemical and structural studies, single-molecule fluorescence
94 resonance energy transfer (FRET) and ensemble kinetic studies provided insights into
95 the molecular mechanisms and kinetics of transcription initiation in the archaeal, RNAP
96 II and RNAP III transcription system⁴³⁻⁵². Interestingly, TBP-DNA complex lifetimes and
97 bending mechanisms differ significantly between the archaeal and eukaryotic system.
98 Archaeal TBP binds and bends the TATA-DNA only transiently⁴⁴. In some archaeal
99 systems, TFB is of crucial importance for the recognition of the promoter by TBP⁴⁴. In
100 all cases, bending is achieved in a single step. Similarly, the interaction of human TBP
101 with the U6 promoter is characterised by short lifetime in the millisecond range⁵² while
102 interaction of yeast TBP with a classical RNAP II promoter is highly stable for minutes
103 to hours and bending occurs in two steps⁴⁴. TFIIIB, e.g., was shown to increase the
104 lifetime of the fully bent state in the RNAP II system. Similarly, the TFIIIB-like factor Brf2
105 prolongs the lifetime of the TBP-DNA complex⁵².

106 Transcription assays as well as smFRET-based DNA bending assays are performed using
107 naked dsDNA of defined length. *In vivo*, however, transcription initiation factors
108 assemble on the promoter DNA in the context of compact nucleosome structures. As a
109 consequence, the transcriptional landscape in eukaryotes is shaped by chromatin
110 remodelling events⁵³. A number of studies analysed the effect of the nucleosome

111 positioning on transcriptional levels and demonstrated that accessibility of the promoter
112 DNA correlates with transcriptional efficiency ⁵⁴. Another regulative aspect of the
113 nucleosome organisation that has to be considered is the topological effects on DNA
114 introduced by tightly spaced nucleosomes ⁵⁵ and the transcription (and replication)
115 machinery. In this context, DNA is subject to mechanical forces. The effect of these
116 forces on transcription initiation, however, has not been analysed as suitable
117 methodological tools were not available so far. Standard force-sensitive methods like
118 magnetic and optical tweezers require long DNA linker strands that connect the DNA
119 under investigation to the macromolecular world, e.g. in magnetical or optical tweezer
120 experimentes a topological change of the investigated DNA can only be transmitted to
121 the beads via this linker. This in turn contributes to a considerable noise in a tweezer
122 experiment. Consequently, subtle changes in DNA topology introduced by DNA-binding
123 proteins like TBP are extremely difficult to detect ⁵⁶.

124 Here, we utilise a recently developed DNA origami-based force clamp ⁵⁷ to monitor the
125 influence of DNA strain on the assembly of transcription initiation factors from the
126 human RNAP II and RNAP III transcription system on the promoter DNA. Our data
127 establishes the RNAPIII - specific initiation factor Bdp1 as the pivotal component of the
128 RNAP III initiation complex that ensures stable anchoring of the initiation factor TFIIIB,
129 and by extension the RNAP III, at the promoter. This exceptional stability provides a
130 stable anchor point for RNAP III at the promoter that's supports the transcription of the
131 short U6, tRNA and 5S rRNAs. Moreover, we demonstrate for the first time that the
132 DNA origami force clamp is a powerful tool to study the force-dependency of complex
133 protein assemblies and that this nanoscopic tool provides detailed mechanistic and
134 kinetic information about biological processes that have not been accessible before.

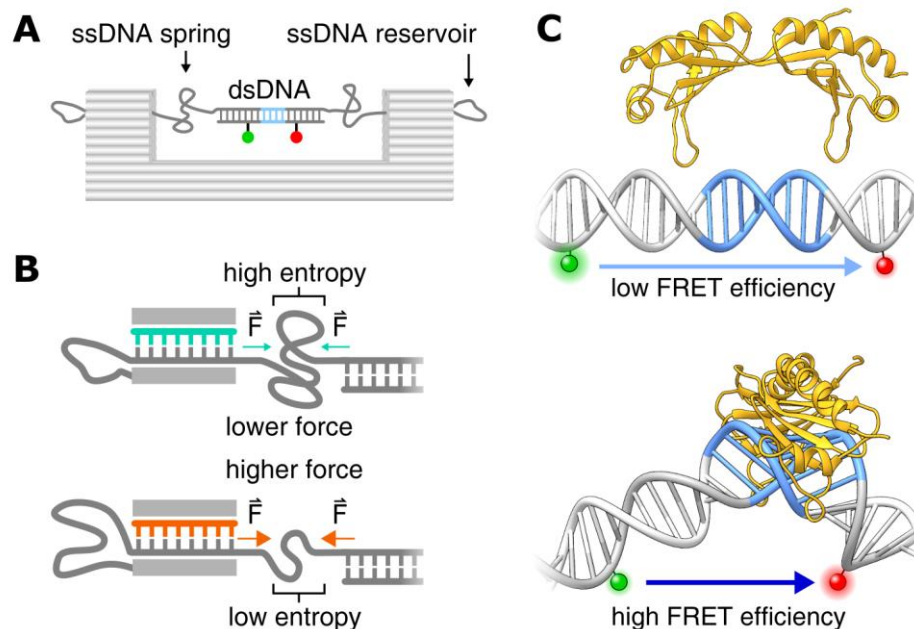
135

136 **Results**

137 **DNA origami-based force clamp to probe force sensitivity of transcription initiation** 138 **complexes**

139 Recently, we introduced a DNA origami-based force clamp that exerts forces in the
140 piconewton regime on a DNA segment (**Figure 1A**)⁵⁷. This nanosized force clamp
141 exploits the entropic spring behaviour of single-stranded DNA (ssDNA) that is placed in
142 the middle of the DNA origami clamp. Forces are tunable by adjusting the length of the
143 ssDNA that is connected to the rigid body of the DNA origami thereby providing two
144 fixed anchor points for the ssDNA (**Figure 1B**). Due to the reduced conformational
145 freedom of a short DNA segment (equivalent with a reduced entropy of the system),
146 higher strain (e.g. force) acts on the DNA. The resulting forces were calculated using a
147 modified freely jointed chain model^{57,58} (for details see **Supplementary Methods**). In
148 this study, we employed DNA origami force clamps with forces ranging from 0 to 6.6
149 pN. The major advantage of the nanoscopic force clamp is that it acts autonomously
150 and does not require a physical connection to a macroscopic instrument. Moreover,
151 the DNA origami force clamp can be produced and used in a highly parallelised manner.
152 In order to study the force-dependency of transcription initiation factor assembly on
153 the promoter DNA, we engineered a prototypical RNAPII (Adenovirus major late
154 promoter, AdMLP) and RNAPIII promoter (human U6 snRNA promoter) sequence into
155 the DNA origami (**Supplementary Figure 1**). The AdMLP promoter contains a TATA-box
156 and BRE element sequence, which are targeted by TBP and TFIIB, respectively. The
157 TATA-box of the U6 snRNA promoter is flanked by the GR-element at position -3/-4 and
158 TD-motif at position +3/+4 relative to the TATA-box (**Supplementary Figure 1**), which
159 are bound by the TFIIB-like factor Brf2⁵². Annealing of a short complementary
160 additional DNA strand that carries a donor (Atto532) and acceptor (Atto647N)
161 fluorophore allows the detection of TBP-induced DNA binding via smFRET
162 measurements (**Figure 1C** and **Supplementary Figure 1**). The correct folding of the DNA
163 nanostructure was verified using transmission electron microscopy (**Supplementary**
164 **Figure 2**). The successful hybridisation of the fluorescently labelled DNA strand is
165 demonstrated by fluorescence correlation spectroscopy measurements as the short
166 dsDNA promoter diffuses seven times faster than the respective DNA origami where

167 the labelled DNA is part of the high molecular weight DNA origami structure
168 (Supplementary Figure 3). We first performed smFRET measurements on freely
169 diffusing DNA origamis and found a single uniform low FRET population for all forces
170 for the AdMLP and U6 promoter force clamps (Figure 2 and 3). The measured FRET
171 efficiencies are in good agreement with FRET efficiencies obtained from linear dsDNA
172 promoter DNAs (Supplementary Figure 4). This demonstrates that the conformation of
173 the promoter DNA is not significantly changed when it is incorporated into the DNA
174 origami force clamp and forces are applied.
175
176



177
178 **Figure 1: DNA-origami based force clamp monitors TBP-induced DNA bending under force. A)**
179 Schematic overview of the DNA origami force clamp. The ssDNA spring protrudes from the DNA origami
180 body and spans the 43 nm gap of the rigid DNA origami clamp body (grey). Centered within the ssDNA
181 spring is a double stranded promoter region incorporating the TATA-box element (blue) flanked by a
182 donor/acceptor (green/red) fluorescent dye pair for FRET sensing. **B)** The ssDNA spring length can be
183 adjusted with DNA from the reservoir by using different staples (teal/orange) during assembly.
184 Reducing the number of nucleotides spanning the gap leads to a smaller number of adoptable
185 conformations of the ssDNA chain and thus results in a higher entropic force. **C)** Single-pair FRET assay
186 as readout for the bending of promoter DNA by the TATA-binding protein (TBP, yellow). A donor (ATTO
187 532, green) and acceptor fluorophore (ATTO 647N, red) flank the TATA-box element (blue) resulting in
188 a low efficiency Förster resonance energy transfer (FRET) between both dyes. Binding of TBP bends the

189 DNA by approximately 90° thereby decreasing the distance between the fluorophors resulting in an
190 increase in FRET efficiency (DNA-TBP structures adapted from: PDB 5FUR).

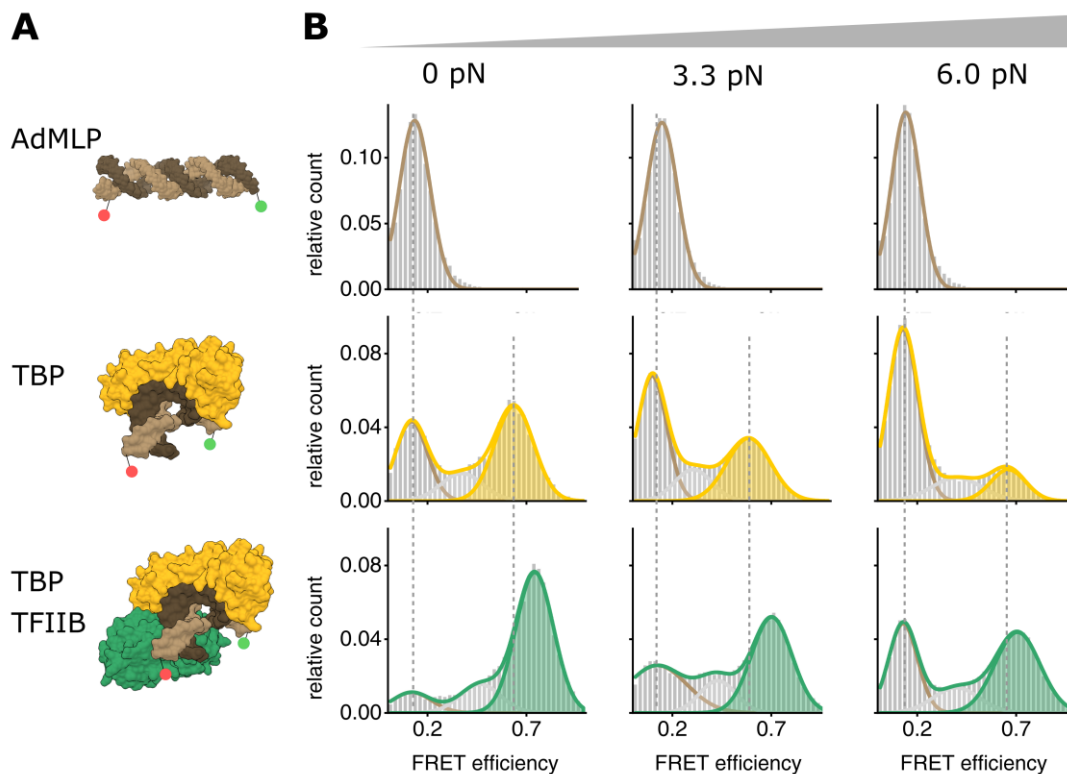
191

192 TBP-induced promoter DNA bending of a Pol II and Pol III promoter under force

193 First, we probed the force-dependency of the human RNAP II transcription initiation
194 complex formation. Basal transcription levels in the RNAPII transcription initiation can
195 be achieved using TBP and TFIIB only. Hence, we added TBP or TBP/TFIIB to the DNA
196 origami force clamp that carries a canonical RNAPII promoter (AdMLP promoter). At
197 the TBP concentration chosen (20 nM), 50% of the molecules showed a high FRET value
198 with a FRET efficiency of 0.63 at 0 pN (**Figure 2, Supplementary Figure 5** and
199 **Supplementary Table 3**). Similar results were obtained using linear dsDNA
200 demonstrating that the DNA origami force clamp is suited to probe TBP-induced DNA
201 bending (**Supplementary Figure 4**). An increase in force to 3.3 and 6.0 pN resulted in a
202 decrease in the fraction of the high FRET population with only 15% of the molecules in
203 the high FRET state at 6.0 pN (**Figure 2, Supplementary Figure 5** and **Supplementary**
204 **Table 3**). These data show that the bending of a RNAP II promoter by TBP is force-
205 dependent. Similarly, addition of human TBP to the U6 promoter DNA origami led to
206 the appearance of a high FRET population ($E = 0.39$) while the fraction of the U6
207 promoter by TBP is reduced at higher forces (**Figure 3**; this data will be discussed in
208 detail below).

209

210



211

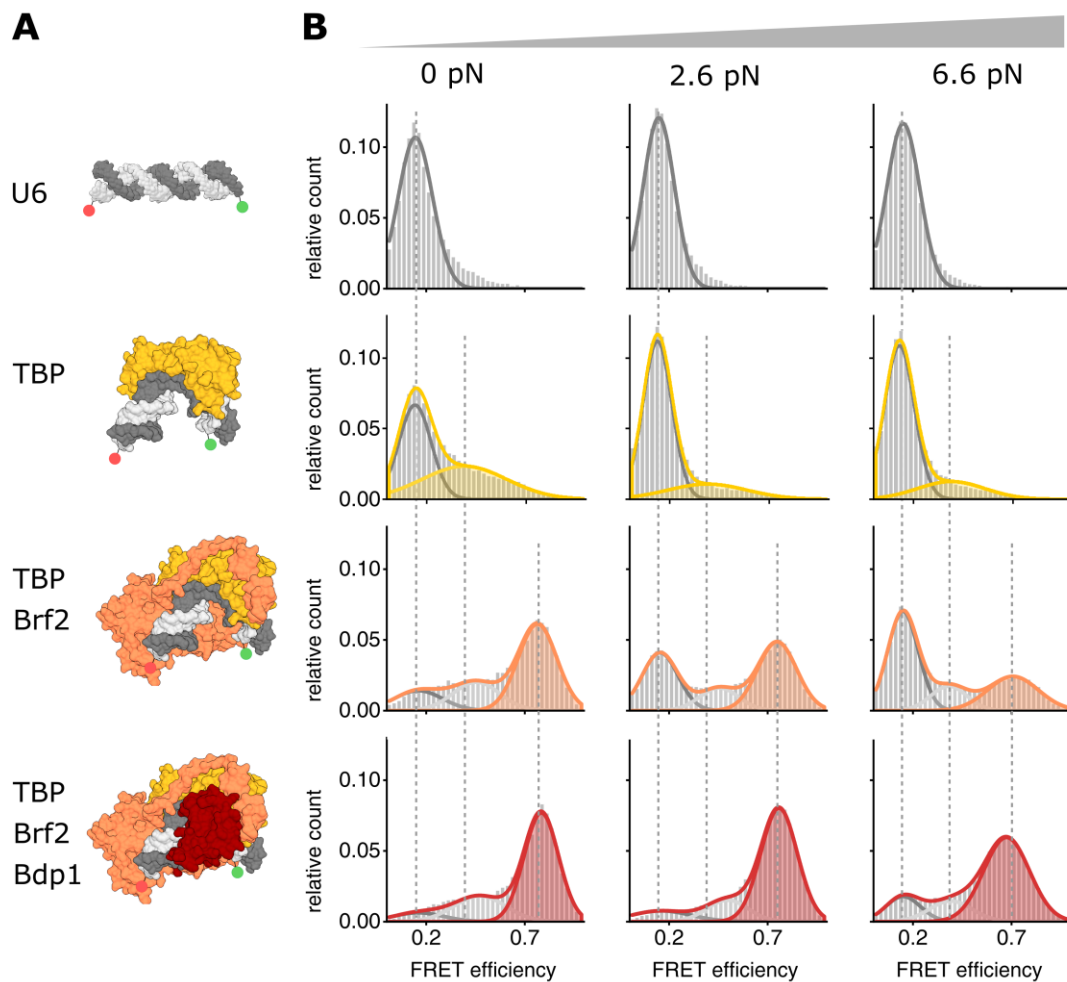
212 **Figure 2: Force dependency of promoter binding of RNA polymerase II initiation factors at a canonical Pol**
 213 **II promoter. A)** Structural model (PDB: 1C9B) of the adenovirus major late promoter (AdMLP, brown) in
 214 an unbent conformation and the 90° bend state bound by TBP (yellow) and TFIIB (green). **B)** Single-
 215 molecule FRET measurements monitor TBP-induced DNA bending after addition of TBP (20 nM) or TBP
 216 and TFIIB (200 nM) to the AdMLP DNA origami force clamps at increasing forces (0, 3.3, 6.0 pN). FRET
 217 efficiency histograms showing the relative distribution between the unbent DNA state (low FRET state,
 218 $E = 0.12$, brown) and TBP-induced bent state (high FRET population, $E = 0.63$ (TBP only, yellow), $E = 0.72$
 219 (TBP/TFIIB, green)). Low and high FRET populations were fitted with a Gaussian distribution. Each
 220 measurement was carried out at least three times. See also **Supplementary Figure 5** and **Supplimentary**
 221 **Table 4.**

222

223 **TFIIB and Brf2/Bdp1 are required to establish fully stable Pol II and Pol III initiation**
 224 **complexes**

225 Addition of TFIIB changes the equilibrium between the bent and unbent DNA state
 226 dramatically. At 0 pN almost all molecules were found in the high FRET state (**Figure 2**).
 227 Increasing the force to 3.3 and 6.0 pN resulted in a decreased high FRET population.
 228 However, at 6.0 pN a significantly higher fraction of molecules (49%) exhibited a high
 229 FRET state as compared to the samples that only contained TBP. Moreover, the high
 230 FRET is shifted to a value of $E = 0.72$ indicating that the bending angle is slightly

231 increased in the presence of TFIIIB. These results suggest that TFIIIB significantly
 232 stabilises the TBP-DNA interaction, which is in agreement with previous smFRET studies
 233 that showed that TFIIIB not only extends the TBP-DNA complex lifetimes but also shifts
 234 the equilibrium towards the fully bent state⁴⁴.



235

236 **Figure 3: Force dependency of promoter binding of RNA polymerase III initiation factors at a canonical**
 237 **Pol III promoter. A)** Structural model (PDB: 5N9G) of the U6 snRNA promoter (U6, dark grey) in an
 238 unbent conformation and the 90° bent state bound by TBP (yellow), TBP+Brf2 (orange) and
 239 TBP+Brf2+Bdp1 (red). **B)** Single-molecule FRET measurements monitor TBP-induced DNA bending after
 240 addition of TBP (20 nM), TBP/Brf2 (20 nM) or TBP/Brf2/Bdp1 (20 nM) to the AdMLP DNA origami force
 241 clamps at increasing forces (0, 2.6, 6.6 pN). FRET efficiency histograms showing the relative distribution
 242 between the unbent DNA state (low FRET state, $E = 0.19$, grey) and TBP-induced bent states in the
 243 absence and presence of additional initiation factors (high FRET population, $E = 0.39$ (TBP only, yellow),
 244 $E = 0.75$ (TBP/Brf2, orange), $E = 0.76$ (TBP/Brf2/Bdp1, red)). Low and high FRET populations were fitted
 245 with a Gaussian distribution. Each measurement was carried out at least three times. See also
 246 **Supplementary Figure 5** and **Supplementary Table 4**.

247

248

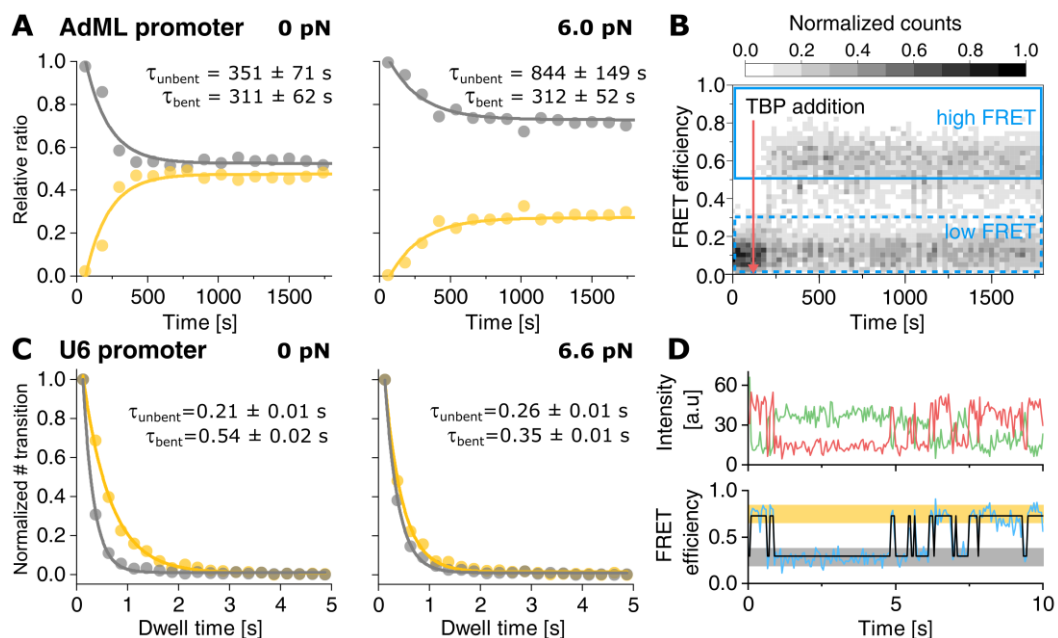
249 Addition of the TFIIB-like factor Brf2 to the TBP-U6 promoter complex also resulted in
250 a stabilisation of the TBP-DNA complex and a shift of the bent DNA population to a
251 higher FRET efficiency ($E = 0.74$). In both cases, however, the complex was still force-
252 sensitive and only a small fraction (Brf2 31%, TFIIB 30%) of molecules was found in the
253 bent state at 6.6 pN (**Figure 2, Supplementary Figure 5**). In previous studies, we
254 observed a significant increase in the lifetime of the complexes when Brf2 was added
255 to the TBP-DNA complex⁵². Addition of Bdp1 to the TBP-Brf2-DNA complex, however,
256 did not substantially affect the complex lifetime when linear promoter DNA was used
257 for smFRET measurements⁵². Hence, we wondered whether Bdp1 influences the
258 complex stability when the DNA experienced increased strain. Probing the force-
259 sensitivity of the TBP-Brf2-Bdp1-DNA complex showed that even at 6.6 pN, the majority
260 of molecules (69%) was found in a bent DNA state. We therefore conclude that in the
261 Pol III system, Bdp1 is the decisive initiation factor that renders the initiation complex
262 fully stable (**Figure 3**). In contrast, TFIIB suffices to ensure such a stable complex
263 formation in the Pol II system.

264

265 **Increased DNA strain destabilises the TBP-DNA interaction**

266 Previous measurements showed that the TBP-DNA interaction is dynamic^{44,52}. This
267 gave us the opportunity to ask whether the increase in strain reduces the lifetime of
268 the TBP-DNA complex (enhanced TBP dissociation with increase in force) or prolongs
269 the lifetime of the unbent DNA state (inhibited TBP association with increase in force).
270 To answer this question, we use two different strategies adapted to the underlying
271 kinetics of association/dissociation process. Slow kinetics in the minutes time regime
272 were measured by acquiring smFRET distributions at different time points after mixing
273 the constituents of the transcription complex. Faster kinetics were measured by
274 monitoring the high-FRET and low FRET state lifetimes directly on single immobilized
275 complexes. Time-resolved smFRET measurements of the TBP-DNA interaction at 0 and
276 6.0 (AdMLP) or 6.6 pN (U6 promoter) showed that the TBP-AdMLP promoter exhibits a
277 lifetime of 311 ± 62 s at 0 pN force while the interaction between TBP and the U6
278 promoter is short-lived ($\tau_{\text{bent}} = 0.54 \pm 0.02$ s) (**Figure 4 and Table S3**). This is in

279 agreement with previous observations using linear dsDNAs⁵². Increased force leads to
 280 an increase in the lifetime of the unbent state while the lifetime of the bent state
 281 remains constant (AdMLP: $\tau_{\text{unbent}} = 844 \pm 149$ s and $\tau_{\text{bent}} = 312 \pm 52$ s). Higher forces do
 282 not influence the lifetime of the unbent state in case of the TBP-U6 promoter DNA
 283 complex (0 pN: $\tau_{\text{unbent}} = 0.21 \pm 0.01$ s, 6.6 pN: $\tau_{\text{unbent}} = 0.26 \pm 0.01$ s). However, the
 284 lifetime of the bent state is slightly reduced at 6.6 pN as compared to 0 pN (0 pN:
 285 $\tau_{\text{bent}} = 0.54 \pm 0.02$ s and $\tau_{\text{bent}} = 0.35 \pm 0.01$ s). These data suggest that two factors
 286 contribute to the reduction of the bent DNA states at higher forces: i) destabilisation
 287 of the TBP-DNA state with increased propability of TBP dissociation from the DNA at
 288 higher forces (spring-loaded TBP ejection mechanism) in case of the U6 promoter and
 289 ii) a decreased propability of the TBP to form a stable complex with DNA (TBP entry
 290 denial) at the AdML promoter. It seems plausible that DNA under strain does provide
 291 less flexibility between the bases for the two phenylalanines pairs to insert into the
 292 DNA and thereby entry of TBP into the DNA is denied. The interaction of the already
 293 inserted phenylalanines with the bases of the DNA, on the other hand, may be reduced
 294 at higher DNA strain, leading to ejection at high strains.
 295



296

297 **Figure 4: Kinetic analysis of the influence of force on TBP-induced DNA-bending. A)** Relative ratios of
 298 low FRET (unbound DNA, grey) to high FRET state (TBP-DNA complex, yellow) in a kinetic experiment
 299 showing the relative fraction of the TBP-DNA complex to the unbent U6 promoter at 0 pN and 6.0 pN.

300 Dwell times were calculated by deconvolution with a perturbation-relaxation model. Data were fitted
301 with a mono-exponential function. **B)** Representative FRET efficiency-time plot of a time course
302 experiment at 0 pN force. TBP (20 nM) was added at 2 min (red arrow). Areas used for calculating the
303 ratio of low and high FRET are indicated by blue boxes. **C)** Dwell-time histograms of the U6 promoter in
304 the unbent (grey) and bent (yellow) state at 0 pN and 6.6 pN force. **D)** Representative donor (green)
305 and acceptor (red) intensity-time trace and the resulting FRET efficiency (blue) fitted with the idealised
306 two-state trace (black) of TBP binding to the U6 promoter at 0 pN force. The low FRET and high FRET
307 states are highlighted in grey and yellow, respectively. Values are given as mean \pm s.e.m. (see also
308 **Supplementary Figure 6 and Table S3**).

309

310

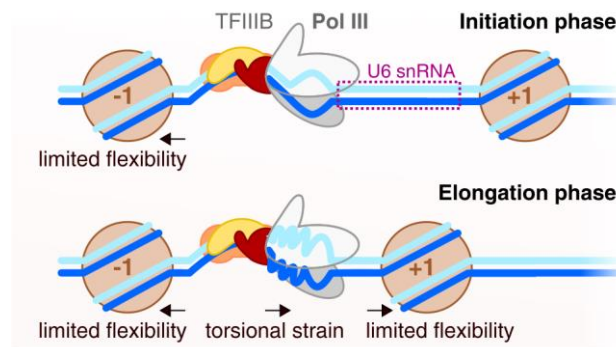
311 Discussion

312 During the initiation phase of transcription, the transcriptional machinery is assembled
313 at the promoter. The minimal factor requirement for transcription initiation consists of
314 TBP and TFIIB to recruit RNAP II and TBP, Brf1 or Brf2 and Bdp1 and additionally SNAPc
315 to recruit RNAP III. One of the interesting questions in this context is why the RNAP III
316 machinery relies on a third basal initiation factor not conserved in the RNAP I or RNAP
317 II system? Based on our data, part of the answer might be found in the fact that
318 promoter DNA - rather than being a rigid stick-like molecule - is part of a complex
319 chromatin superstructure with dynamic structural variability and consequently subject
320 to mechanical forces in the dynamic landscape of chromatin that is constantly exposed
321 to changes by chromatin remodelers and gene activators⁵⁴. This also includes loop
322 formation and tight nucleosomal packaging that exerts mechanical forces on the DNA
323^{59,60}. Additionally, attractive interaction between nucleosomes mediated by the histone
324 tail domains have recently been observed using DNA nanotechnology⁵⁵. These close-
325 range interactions vary in strength between -0.3 to -8 kcal/mol which falls into the
326 range covered by our experiments^{55,61-64} (**Supplementary Figure 7**). However, the
327 chromatin landscape and consequently the forces that act on the promoter DNA differ
328 between Pol II and III promoters. In this work, we investigated the force sensitivity of
329 transcription initiation factor assembly at the promoter DNA at variable forces
330 employing a novel method to carry out force measurements based on a DNA origami
331 force clamp⁵⁷. Combined with a smFRET assay, we were able to quantify TBP-induced
332 promoter DNA bending and to evaluate the influence of additional initiation factors.
333 Using identical TBP concentrations, we found that human TBP bends the U6 snRNA
334 promoter less efficiently under force than the AdML promoter. This is not surprising as
335 only four out of eight bases of the TATA sequence of the U6 promoter sequence match
336 the human consensus TATA box sequence⁹. In contrast, the AdMLP provides a perfect
337 TATA box. This is also reflected in the bent/unbent state lifetime measured for both
338 complexes (Figure 4). Here, mainly the unbent state lifetime increases with force, thus
339 the AdMLP-TBP complex with its higher lifetime is less effected than the transient U6-
340 TBP complex. Our data show that TBP in conjunction with TFIIB forms stable and force-
341 resistant complexes at the prototypical RNAP II AdML promoter. The long lifetime of

342 the TBP-DNA complex, the observed stabilising effect of TFIIB and the increase in
343 bending angle upon addition of TFIIB is consistent with previous smFRET
344 measurements using yeast TBP/TFIIB ⁴⁴. In the RNAP III transcription system, we
345 observed that the TFIIB-like factor Brf2 also enhances the stability of the TBP-DNA
346 complex ⁵². Interestingly, the addition of the third initiation factor, Bdp1, yields an
347 outstandingly stable initiation complex at the U6 promoter. It is noteworthy that the
348 spliceosomal U6 RNA and other RNAP III gene products are highly expressed. This in
349 turn requires robust formation of initiation complexes at the promoter as
350 transcriptional regulation cannot take place at the level of elongation at these
351 extremely short genes. Hence, the RNAP III-exclusive initiation factor Bdp1 plays a
352 decisive role in transcription initiation as it allows the maintenance of fully assembled
353 TFIIB - promoter DNA complex. The stable anchoring of initiation proteins as well as
354 the RNAP III is furthermore of crucial importance as RNAP III is thought to undergo
355 extensive cycles of facilitated re-initiation ⁶⁵⁻⁶⁷. RNAP III only transcribes very short
356 RNAs (5S rRNA, tRNAs, U6 snRNA) and biochemical and recent structural data suggest
357 that RNAP III, in contrast to RNAP II, might not escape from the promoter during
358 transcription elongation but possibly remains bound to the promoter and re-initiates
359 directly after termination ^{65,67 66,68}. Hence, initiation factors at the promoter are
360 situated at a DNA section that is topological restrained on the one hand side by the -1
361 nucleosome, which is stably positioned at -150 bp ⁶⁹ and a firmly associated
362 transcribing RNA polymerase. Upon promoter opening of the DNA by RNAP III in
363 concert with Bdp1, the DNA section experiences torsional strain as the DNA is unwound
364 and the strain cannot be released due to the static nucleosome and RNAP III that
365 represent fixed boundaries (**Figure 5**). Hence, TFIIB is likely to experience mechanical
366 forces that are compensated by the extremely stable initiation complex. Moreover, in
367 a model where the polymerase remains bound to the promoter, strain would build up
368 during transcription between the promoter binding site and the active site due to the
369 increasing amount of transcribed DNA that has to be accommodated in the
370 polymerase. This additionally increases the forces that the transcription initiation
371 complex has to withstand.

372

373



374

375 **Figure 5: Model describing the role of DNA strain in RNA polymerase III initiation complexes.**

376 On the U6 snRNA promoter, the -1 nucleosome is firmly positioned close to the upstream promoter
377 region, limiting DNA flexibility. Continuous transcription of the U6 snRNA by promoter-bound RNA
378 polymerase III creates torsional strain. The +1 nucleosome is positioned downstream of the gene body.
379 Proteins and nucleic acids are color coded as follows: TBP (yellow), TFIIB (green), Brf2 (orange), Bdp1
380 (red), RNA polymerase II/III (grey), nucleosome (brown), template strand (blue), non-template strand
381 (cyan).

382

383 The situation is different at RNAP II promoters as RNAP II transcribes mRNAs that can
384 be hundreds of basepairs in length and re-initiation does not seem to play a role.
385 Another point to consider is that RNAP II and III promoters display a nucleosome
386 depleted region around the transcription start site (TSS) but a conserved +1
387 nucleosome is found at position +40 in genes with elongating RNAP and +10 in silent
388 genes (RNAP II)^{70,71} and 220 bp (RNAP III)⁶⁹. As the position of the +1 nucleosome does
389 not show a strong sequence-dependency and its position appears to be flexible when
390 nucleosomes are reconstituted on naked DNA *in vitro*⁷¹, it has been speculated that
391 initiation factors situated at the promoter help to establish the position of the +1
392 nucleosome^{54,72}. This might be especially relevant for RNAP II genes where the +1
393 nucleosome is found in close proximity to the TSS. In this case, initiation factors need
394 to be stably attached at the promoter in order to avoid displacement by the
395 nucleosome. Here, TFIIB acts as the initial stabilising factor at RNAP II promoters to
396 secure TBP at the DNA and this minimal initiation complex can be further extended by
397 additional initiation factors like TFIIA and ultimately extended to include the Mediator
398 complex¹⁹. Homologues factors are not found in the RNAP III system but our studies
399 show that the addition of Bdp1 to the RNAP III initiation factor lineup is necessary and

400 sufficient to maintain an active initiation complex even when the transcribing RNAP III
401 potentially causes increased DNA strain in the promoter DNA. Interestingly, extending
402 the initial TBP-DNA complex by additional transcription factors increases the lifetime of
403 the unbent state increases with force. This indicates that the tension on the DNA is a
404 mechanism of gene regulation. The packaging, histone placement, action of the
405 replication machinery and binding of regulatory proteins will certainly have an impact
406 on the tension that the initiation complex is exposed to. Thus, besides steric effects,
407 tension influences transcription. On the other hand, after the transcription initiation
408 complex has formed (i.e. more than one transcription factor is assembled at the
409 promoter), the lifetime of the complex becomes independent of force. This might
410 indicate that after the decision for transcription was taken, the process should become
411 independent of mechanical factors ensuring that the RNA polymerase enters the
412 elongation phase of transcription.

413

414 **Material and Methods**

415 **Proteins**

416 All proteins were expressed and purified as described previously⁵². For the
417 measurements shown we used a N-terminal Bdp1 variant that encompasses residues
418 130-484 that efficiently forms a complex composed of TBP, Brf2 and promoter
419 DNA^{21,52}.

420

421 **Cloning of promoter DNA sequences into the M13 DNA origami scaffold**

422 The Force-clamp origami used in this work is based on the M13mp18 ssDNA. The
423 multicloning site of the ssDNA phage DNA is located within the spring region of the
424 force clamp, and the two different RNA polymerase promoters were cloned between
425 the BamHI- HindIII restriction sites of the multicloning site. AdMPL promoter and U6sn
426 RNA promoters were assembled by means of hybridisation of 5'-phosphorylated
427 forward and reverse oligonucleotides (**Supplementary Table 1**). Annealing of the
428 forward and reverse oligonucleotides generate BamHI and HindIII sticky ends. Cloning
429 was performed using the replicative form (dsDNA) of the M13 phage, and high titer
430 phage stocks and ssDNA M13 DNA for DNA origami assembly were prepared as
431 described elsewhere^{73,74}. In both cases, promoter sequences were confirmed by
432 sequencing after cloning.

433

434 **Preparation of doubly labelled single-stranded DNAs**

435 Doubly labelled single-stranded DNAs were prepared from individual DNA strands that
436 carry either the donor or the acceptor fluorophore (**Supplementary Table 1**). The final
437 DNA strand carries both dyes and is complementary to the promoter region of the
438 origami scaffold. 10 μ M of the appropriate donor strand (**_D**), acceptor strand (**_A**) and
439 complementary ligation strand (**_Lig**) were hybridised in 100 μ L annealing buffer (Tris
440 HCl pH 8.0, 150 mM NaCl), heated to 90 °C for 3 min and cooled down to 20 °C over
441 2 h. For the ligation, 20 μ L 10x T4 ligase buffer (NEB), 70 μ L Millipore water and 10 μ L
442 T4 DNA ligase (NEB) were added to the hybridization reaction and incubated for 60 min
443 at 20 °C.

444 In order to purify the ligated single strand DNA, the DNA was separated on a 200 μ L
445 preparative denaturing TBE gel (15% (v/v) acrylamide/bisacrylamid (19:1), 6 M urea).
446 To this end, RNA loading buffer (47.5 % glycerol (v/v) 0.1 % (v/v) SDS, 0.5 mM EDTA)
447 was added to the ligation reaction and the sample was heated to 80°C and cooled on
448 ice. The DNA was separated at 200 V over 40 min. The gel was visualized under UV-light
449 and the band corresponding to the doubly labelled DNA strand was excised and
450 pulverized. DNA was extracted by adding 1 mL of 1x TBE buffer and shaking at 4 °C for
451 2h. The gel debris was pelleted via centrifugation at 15000 rcf for 30 min (repeated
452 once). The DNA was precipitated by addition of 1/10 volume of ammonium acetate
453 solution (3 M, pH 5) and 2.5 volumes of ethanol. The sample was incubated at -80 °C
454 for 1 h followed by a centrifugation step for 1 h at 4 °C. The supernatant was carefully
455 decanted and the DNA was washed by addition of 5 mL of 70% ethanol and 30 min
456 centrifugation at 15000 rcf. The supernatant was completely removed, the pellet dried
457 for 10 min at 20 °C and resuspended in 10 mM Tris HCl pH 8.0 +50 mM NaCl.

458

459 **DNA origami preparation and purification**

460 DNA origamis were assembled as described previously ⁵⁷. In brief, scaffold DNA
461 (25 nM), core staple strands (200 nM), force staple strands (400 nM), biotin adapter
462 staple strands (200 nM) and the complementary doubly labelled promoter DNA strand
463 (200 nM) were mixed in folding buffer (10 mM Tris pH 7.6, 1 mM EDTA, 20 mM MgCl₂,
464 5 mM NaCl) and subjected to a multistep thermocycler protocol (**Supplementary**
465 **Table 2**). Afterwards, the origami was purified by addition of one volume of
466 2x precipitation puffer (Tris HCl pH 7.6, 1 mM EDTA, 500 mM NaCl, 15% (w/v) PEG-
467 8000) and centrifugation at 20000 rcf for 30 min at 4 °C. Afterwards, the supernatant
468 was decanted and the pellet resuspended in 30 μ L folding buffer for 30 min at 30 °C
469 under constant shaking. All purification steps were repeated once.

470

471

472 **Restriction digestion of origami scaffolds**

473 In order to generate force clamps with 0 pN force the spring strand was cleaved with a
474 BamHI restriction endonuclease. To this end, 200 μ M of the scaffold DNA and 3x molar
475 excess of BamHI_comp strand were hybridized in FastDigest Green buffer (Thermo
476 Scientific) by heating the sample to 90 °C followed by gradual cooling to 20 °C over 2 h.
477 Afterwards, 1 U of FastDigest BamHI (Thermo Scientific) was added, incubated at 37 °C
478 for 4 h. Subsequently, BamHI was heat inactivated at 80 °C for 10 min.

479

480 **Surface preparation**

481 Silica microscope slides used for TIRF experiments were prepared as described
482 before⁵². Briefly, fused silica slides (Plano) were cleaned in peroxomonsulfuric acid (70%
483 (v/v) sulfuric acid; Fisher Scientific, 10% (v/v) hydrogen peroxide; Sigma-Aldrich) for 30
484 min and washed with Millipore water under sonication. Afterwards, the slides were
485 incubated in methanol for 20 min and sonicated for 5 min. For silan passivation, the
486 slides were incubated in a freshly prepared N-[3-(Trimethoxysilyl)propyl]ethyldiamine
487 (Sigma-Aldrich) solution (2% (v/v) in methanol with 4% (v/v) acetic acid) for 20 min,
488 rinsed with methanol five times and an additional 20 times with Millipore water. The
489 slides were dried for 1h at 37 °C. For polyethylene glycole (PEG) passivation, 100 μ L of
490 freshly prepared passivation solution (200 mg/mL methoxy-PEG succinimidyl valerate
491 5000 (Laysan Bio), 5 mg/mL biotin-PEG (Laysan Bio) in 1 mM NaHCO₃) was sandwiched
492 between a slide and a coverslip, incubated for 2 h and rinsed with Millipore water 20
493 times. The slides and coverslips were fully dried at 37 °C, vacuum-sealed in plastic tubes
494 and stored at -20 °C.

495

496 **TIRF immobilisation assay**

497 Single-molecule FRET measurements on immobilized DNA/protein complexes were
498 carried out in custom-built flow-chambers based on fused silica slides passivated with
499 polyethylene glycole (PEG). Flow chambers were prepared and assembled a described
500 before⁴⁴.

501 For fluorescence measurements the flow chamber was incubated with 0.1 mg/mL
502 NeutrAvidin (Pierce) in 1 x TBS (125 mM Tris/HCl pH 8, 150 mM NaCl) for 5 min and

503 washed with 500 μ L T78 buffer (100 mM Tris/HCl pH 7.8, 60 mM KCl, 5 mM MgCl₂,
504 0.5 mg/mL BSA, 1% (v/v) glycerol). Afterwards, the chamber was flushed with DNA
505 origami force clamps (10 pM in folding buffer) for 5 s and washed with 500 μ L T78
506 buffer. The chamber was flushed with photostabilizer buffer (T78 buffer with 2 mM
507 Trolox, 1% (w/v) D-glucose, 7.5 U/mL glucose oxidase type VII (Sigma Aldrich), 1 kU/mL
508 catalase (Sigma Aldrich)) supplemented with 10 nM human TBP and incubated for 5
509 min before starting video acquisition.

510

511 **Wide-field single-molecule detection and data analysis**

512 Time resolved single-molecule fluorescence measurements were performed on a
513 homebuilt prism-type total internal reflection setup based on a Leica DMI8 inverse
514 research microscope. Fluorophores were excited with a 532 nm solid state laser
515 (Coherent OBIS) with a power of 30 mW and 637 nm diode laser (Coherent OBIS, clean-
516 up filter ZET 635/10, AHF Göttingen) with a power of 50 mW employing alternating
517 laser excitation (Multistream, Cairn Research, UK)⁷⁵. The fluorescence was collected
518 by a Leica HC PL Apo 63x N.A. 1.20 water-immersion objective and split by wavelength
519 with a dichroic mirror (HC BS 640, AHF) into two detection channels that were further
520 filtered with a 582/75 bandpass filter (Brightline HC, AHF) in the green channel and a
521 635 nm long-pass filter (LP Edge Basic, AHF) in the red detection channel. Both
522 detection channels were recorded by one EMCCD camera (Andor IXon Ultra 897, EM-
523 gain 20, framerate 40 Hz, 400 frames) in a dual-view configuration (TripleSplit, Cairn
524 Research).

525 The videos were analysed employing the iSMS software⁷⁶ using the programs defaults
526 settings. Molecule spots were detected using a threshold of 100 for ATTO 532 and
527 ATTO 647N spots. FRET efficiencies were calculated as proximity ratios from
528 fluorescence intensity time traces that were corrected for background fluorescence
529 using the average intensity of all pixels with a 2 pixel distance to the molecule spot.

530 For TBP dwell time histograms, traces showing dynamic switching between FRET states
531 were fitted with the vbFRET algorithm⁷⁷ limited to two states.

532 FRET efficiency histograms were calculated from all frames of traces showing dynamic
533 switching between states with an S-value between 0.4 to 0.6 and were fitted with a

534 Gaussian distribution. All states calculated with vbFRET with a FRET efficiency within
535 the FWHM of a fitted FRET population were used to calculate the dwell time histogram.
536 The histograms of at least three independent experiments were normalized and fitted
537 with a monoexponential decay function to calculate the mean dwell time in the high
538 FRET state (TBP bound to DNA).

539

540 **Confocal Single-pair FRET measurements**

541 Prior to sample loading, the sample chambers (Cellview slide, Greiner Bio-One) were
542 passivated with 10 mM Tris/HCl pH 8 with 2 mg/mL BSA for 10 min and washed once
543 with T78 buffer.

544 For equilibrium measurements (**Figure 2, Figure 3, Supplementary Figure 4**) complexes
545 were formed with 20 pM DNA origami and 20 nM TBP, Brf2 and Bdp1 or 200 nM TFIIB
546 and incubated for 30 min at room temperature in T78 buffer with 2 mM DTT.

547 For time course experiments (**Figure 4, Supplementary Figure 6**) 20 pM DNA origami
548 and 20 nM Brf2 and Bdp1 or 200 nM of TFIIB in T78 buffer with 2 mM DTT were added
549 to the sample chamber and data acquisition was started to measure the unbound DNA
550 state. After 2 minutes, TBP was added to initiate complex formation.

551 Single-molecule fluorescence of diffusing complexes was detected with a
552 MicroTime 200 confocal microscope (Picoquant) equipped with pulsed laser diodes
553 (532 nm: LDH-P-FA-530B; 636 nm: LDH-D-C-640; PicoQuant / cleanup filter: zet635;
554 Chroma). The fluorophors were excited at 20 μ W using pulsed interleaved excitation.
555 Emitted fluorescence was collected using a 1.2 NA, \times 60 microscope objective
556 (UplanSApo \times 60/1.20W; Olympus) and a 50- μ m confocal pinhole. A dichroic mirror
557 (T635lpxr; Chroma) separated donor and acceptor fluorescence. Additional bandpass
558 filters (donor: ff01-582/64; Chroma; acceptor: H690/70; Chroma) completed spectral
559 separation of the sample fluorescence. Each filtered photon stream was detected by
560 an individual APD (SPCM-AQRH-14-TR, Exceliatas Technologies) and analyzed by a
561 TCSPC capable PicoQuant HydraHarp 400.

562

563 **Data analysis**

564 Data analysis of confocal FRET measurements was performed with the software
565 package PAM⁷⁸. Photon bursts of diffusing molecules were determined by an all-
566 photon burst search (APBS, parameters: $L=50$, $M=20$, and $T=500 \mu\text{s}$) and an additional
567 dual-channel burst search (DCBS, parameters: $L=50$, $M_{GG+GR}=20$, $M_{RR}=20$, and
568 $T=500 \mu\text{s}$). Burst data were corrected for donor leakage and direct excitation of the
569 acceptor (determined from APBS according to ⁷⁹) as well as γ and β (determined from
570 DCBS ES-histograms using an internal fit on multiple E/S separated FRET populations).
571 The data were binned (bin size =0.025), plotted as E histogram and fitted with a single
572 (DNA) or triple Gaussian fit.

573

574 **Kinetics measurements**

575 Data were processed as above. All bursts were sorted according to their FRET efficiency
576 (low FRET for $E<0.3$ and high FRET for $E>0.6$) and binned by macrotime (bin size=2 min).
577 Low FRET and high FRET bins were normalized to the combined sum to determine
578 relative ratios of both populations which were plotted against time and fitted with a
579 mono-exponential function. The fit-derived decay constant and y-offset (y_0 , equivalent
580 to low FRET ratio at equilibrium) for the low FRET population were used to determine
581 dwell times in the high FRET and low FRET state via deconvolution with a perturbation-
582 relaxation model (see also **Supplementary informations**).

583

584

585 **Acknowledgements**

586 We gratefully acknowledge financial support by the Deutsche Forschungsgemeinschaft
587 (SFB960-TP7 to D.G.). PT acknowledges support by the DFG (grant INST 86/1904-1
588 FUGG), excellence clusters CIPSM (Center for Integrated Protein Science Munich) and
589 NIM (Nanosystems Initiative Munich). TL is also supported through NIM and the
590 SFB1032-TP6. FH and CE were supported by DFGs 'Emmy-Noether-Programm' [DFG
591 grant no. EN 1204/1-1] and and SFB960-TP A8. A.V. is supported by a Cancer Research
592 UK Programme Foundation (CR-UK C47547/A21536) and a Wellcome Trust Investigator
593 Award (200818/Z/16/Z).

594 Furthermore, we would like to thank Dr. Sarah Willkomm for advice on analysing the
595 kinetics data, Michael PilsI for support on the EM measurements and Elisabeth
596 Piechatschek and Elke Papst for technical assistance.

597

598 **Author contributions**

599 D.G. and K.K. conceived the study. K.K. performed the single-molecule measurements.
600 K.K. and T.S. analyzed the single-molecule data. J.G. and A.V. purified the proteins. T.S.,
601 A.M.V., T. L. and P. T. designed and manufactured the DNA origami force clamp. F.H.
602 and C.E. carried out electron microscopy measurements and analysed the data. K.K.
603 and D.G. wrote the paper. All authors commented on the paper.

604

605

606

607

- 608 1. Werner, F. & Grohmann, D. Evolution of multisubunit RNA polymerases in the three
609 domains of life. *Nature reviews. Microbiology* **9**, 85–98; 10.1038/nrmicro2507
610 (2011).
- 611 2. Dienemann, C., Schwalb, B., Schilbach, S. & Cramer, P. Promoter Distortion and
612 Opening in the RNA Polymerase II Cleft. *Molecular cell* **73**, 97-106.e4;
613 10.1016/j.molcel.2018.10.014 (2019).
- 614 3. Griesenbeck, J., Tschochner, H. & Grohmann, D. Structure and Function of RNA
615 Polymerases and the Transcription Machineries. *Sub-cellular biochemistry* **83**, 225–
616 270; 10.1007/978-3-319-46503-6_9 (2017).
- 617 4. Liu, X., Bushnell, D. A., Wang, D., Calero, G. & Kornberg, R. D. Structure of an RNA
618 polymerase II-TFIIB complex and the transcription initiation mechanism. *Science*
619 (*New York, N.Y.*) **327**, 206–209; 10.1126/science.1182015 (2010).
- 620 5. Sainsbury, S., Niesser, J. & Cramer, P. Structure and function of the initially
621 transcribing RNA polymerase II–TFIIB complex. *Nature* **493**, 437–440;
622 10.1038/nature11715 (2012).
- 623 6. Kramm, K., Engel, C. & Grohmann, D. Transcription initiation factor TBP: old friend
624 new questions. *Biochemical Society Transactions* **47**, 411–423;
625 10.1042/BST20180623 (2019).
- 626 7. Vannini, A. & Cramer, P. Conservation between the RNA polymerase I, II, and III
627 transcription initiation machineries. *Molecular cell* **45**, 439–446;
628 10.1016/j.molcel.2012.01.023 (2012).
- 629 8. Engel, C., Neyer, S. & Cramer, P. Distinct Mechanisms of Transcription Initiation by
630 RNA Polymerases I and II. *Annual review of biophysics* **47**, 425–446;
631 10.1146/annurev-biophys-070317-033058 (2018).
- 632 9. Basehoar, A. D., Zanton, S. J. & Pugh, B.F. Identification and Distinct Regulation of
633 Yeast TATA Box-Containing Genes. *Cell* **116**, 699–709; 10.1016/S0092-
634 8674(04)00205-3 (2004).
- 635 10. Savinkova, L. *et al.* An Experimental Verification of the Predicted Effects of Promoter
636 TATA-Box Polymorphisms Associated with Human Diseases on Interactions
637 between the TATA Boxes and TATA-Binding Protein. *PLoS ONE* **8**, e54626;
638 10.1371/journal.pone.0054626 (2013).

- 639 11. Wobbe, C. R. & Struhl, K. Yeast and human TATA-binding proteins have nearly
640 identical DNA sequence requirements for transcription in vitro. *Molecular and*
641 *cellular biology* **10**, 3859–3867; 10.1128/MCB.10.8.3859.Updated (1990).
- 642 12. Smollett, K., Blombach, F., Reichelt, R., Thomm, M. & Werner, F. A global analysis of
643 transcription reveals two modes of Spt4/5 recruitment to archaeal RNA
644 polymerase. *Nature Microbiology* **2**, 17021; 10.1038/nmicrobiol.2017.21 (2017).
- 645 13. Krebs, A. R. *et al.* Genome-wide Single-Molecule Footprinting Reveals High RNA
646 Polymerase II Turnover at Paused Promoters. *Molecular cell* **67**, 411 - 422.e4;
647 10.1016/J.MOLCEL.2017.06.027 (2017).
- 648 14. Kim, T. H. *et al.* A high-resolution map of active promoters in the human genome.
649 *Nature* **436**, 876–880; 10.1038/nature03877 (2005).
- 650 15. Kim, J. L., Nikolov, D. B. & Burley, S. K. Co-crystal structure of TBP recognizing the
651 minor groove of a TATA element. *Nature* **365**, 520–527; 10.1038/365520a0 (1993).
- 652 16. Kim, Y., Geiger, J. H., Hahn, S. & Sigler, P. B. Crystal structure of a yeast TBP/TATA-
653 box complex. *Nature* **365**, 512–520; 10.1038/365512a0 (1993).
- 654 17. Kosa, P. F., Ghosh, G., DeDecker, B. S. & Sigler, P. B. The 2.1-Å crystal structure of
655 an archaeal preinitiation complex: TATA-box-binding protein/transcription factor
656 (II)B core/TATA-box. *Proceedings of the National Academy of Sciences of the United*
657 *States of America* **94**, 6042–6047; 10.1073/PNAS.94.12.6042 (1997).
- 658 18. Kostrewa, D. *et al.* RNA polymerase II–TFIIB structure and mechanism of
659 transcription initiation. *Nature* **462**, 323–330; 10.1038/nature08548 (2009).
- 660 19. Hantsche, M. & Cramer, P. Conserved RNA polymerase II initiation complex
661 structure. *Current Opinion in Structural Biology* **47**, 17–22;
662 10.1016/j.sbi.2017.03.013 (2017).
- 663 20. He, Y. *et al.* Near-atomic resolution visualization of human transcription promoter
664 opening. *Nature* **533**, 359–365; 10.1038/nature17970 (2016).
- 665 21. Abascal-Palacios, G., Ramsay, E. P., Beuron, F., Morris, E. & Vannini, A. Structural
666 basis of RNA polymerase III transcription initiation. *Nature* **553**, 301–306;
667 10.1038/nature25441 (2018).

- 668 22. Sadian, Y. *et al.* Structural insights into transcription initiation by yeast RNA
669 polymerase I. *The EMBO Journal* **36**, 2698–2709; 10.15252/embj.201796958
670 (2017).
- 671 23. Vorländer, M. K., Khatter, H., Wetzell, R., Hagen, W. J.H. H. & Müller, C. W. Molecular
672 mechanism of promoter opening by RNA polymerase III. *Nature* **553**, 295–300;
673 10.1038/nature25440 (2018).
- 674 24. Sainsbury, S., Bernecky, C. & Cramer, P. Structural basis of transcription initiation by
675 RNA polymerase II. *Nature Reviews Molecular Cell Biology* **16**, 129–143;
676 10.1038/nrm3952 (2015).
- 677 25. Hausner, W., Wettach, J., Hethke, C. & Thomm, M. Two transcription factors related
678 with the eucaryal transcription factors TATA-binding protein and transcription
679 factor IIB direct promoter recognition by an archaeal RNA polymerase. *The Journal*
680 *of biological chemistry* **271**, 30144–30148; 10.1074/JBC.271.47.30144 (1996).
- 681 26. Werner, F. & Weinzierl, R. O. J. A recombinant RNA polymerase II-like enzyme
682 capable of promoter-specific transcription. *Molecular cell* **10**, 635–646 (2002).
- 683 27. Buratowski, S., Hahn, S., Guarente, L. & Sharp, P. A. Five intermediate complexes in
684 transcription initiation by RNA polymerase II. *Cell* **56**, 549–561; 10.1016/0092-
685 8674(89)90578-3 (1989).
- 686 28. Cavallini, B., Huet, J., Plassat, J. L., Sentenac, A. & Egly, J. M. A yeast activity can
687 substitute for the HeLa cell TATA box factor. *Nature* **334**, 77–80; 10.1038/334077a0
688 (1988).
- 689 29. Bell, S. D. & Jackson, S. P. The Role of Transcription Factor B in Transcription
690 Initiation and Promoter Clearance in the Archaeon *Sulfolobus acidocaldarius*.
691 *Journal of Biological Chemistry* **275**, 12934–12940; 10.1074/jbc.275.17.12934
692 (2000).
- 693 30. Khatter, H., Vorländer, M. K. & Müller, C. W. RNA polymerase I and III: similar yet
694 unique. *Current Opinion in Structural Biology* **47**, 88–94; 10.1016/j.sbi.2017.05.008
695 (2017).
- 696 31. Eberhard, D., Tora, L., marc Egly, J. & Grummt, I. A TBP-containing multiprotein
697 complex (TIF-IB) mediates transcription specificity of murine RNA polymerase I.
698 *Nucleic Acids Research* **21**, 4180–4186; 10.1093/nar/21.18.4180 (1993).

- 699 32. Steffan, J. S., Keys, D. A., Dodd, J. A. & Nomura, M. The role of TBP in rDNA
700 transcription by RNA polymerase I in *Saccharomyces cerevisiae*: TBP is required for
701 upstream activation factor- dependent recruitment of core factor. *Genes and*
702 *Development* **10**, 2551–2563; 10.1101/gad.10.20.2551 (1996).
- 703 33. Siddiqi, I., Keener, J., Vu, L. & Nomura, M. Role of TATA binding protein (TBP) in
704 yeast ribosomal dna transcription by RNA polymerase I: defects in the dual
705 functions of transcription factor UAF cannot be suppressed by TBP. *Molecular and*
706 *cellular biology* **21**, 2292–2297; 10.1128/MCB.21.7.2292-2297.2001 (2001).
- 707 34. Keener, J., Dodd, J. A., Lalo, D. & Nomura, M. Histones H3 and H4 are components
708 of upstream activation factor required for the high-level transcription of yeast rDNA
709 by RNA polymerase I. *Proceedings of the National Academy of Sciences of the United*
710 *States of America* **94**, 13458–13462; 10.1073/PNAS.94.25.13458 (1997).
- 711 35. Bedwell, G. J., Appling, F. D., Anderson, S. J. & Schneider, D. A. Efficient transcription
712 by RNA polymerase I using recombinant core factor. *Gene* **492**, 94–99;
713 10.1016/j.gene.2011.10.049 (2012).
- 714 36. Keener, J., Josaitis, C. A., Dodd, J. A. & Nomura, M. Reconstitution of yeast RNA
715 polymerase I transcription in vitro from purified components: TATA-binding protein
716 is not required for basal transcription. *Journal of Biological Chemistry* **273**, 33795–
717 33802; 10.1074/jbc.273.50.33795 (1998).
- 718 37. Schramm, L. & Hernandez, N. Recruitment of RNA polymerase III to its target
719 promoters. *Genes & Development* **16**, 2593–2620; 10.1101/gad.1018902 (2002).
- 720 38. Kassavetis, G. A. A minimal RNA polymerase III transcription system. *The EMBO*
721 *Journal* **18**, 5042–5051; 10.1093/emboj/18.18.5042 (1999).
- 722 39. Verma, N. *et al.* Bdp1 interacts with SNAPc bound to a U6, but not U1, snRNA gene
723 promoter element to establish a stable protein-DNA complex. *FEBS Letters* **592**,
724 2489–2498; 10.1002/1873-3468.13169 (2018).
- 725 40. Kassavetis, G. A. & Geiduschek, E. P. Transcription factor TFIIIB and transcription by
726 RNA polymerase III. *Biochemical Society Transactions* **34**, 1082–1087;
727 10.1042/BST0341082 (2006).
- 728 41. Schramm, L., Pendergrast, P. S., Sun, Y. & Hernandez, N. Different human TFIIIB
729 activities direct RNA polymerase III transcription from TATA-containing and TATA-

- 730 less promoters. *Genes and Development* **14**, 2650–2663; 10.1101/gad.836400
731 (2000).
- 732 42. Kassavetis, G. A., Braun, B. R., Nguyen, L. H. & Geiduschek, E. P. S. cerevisiae TFIIIB
733 is the transcription initiation factor proper of RNA polymerase III, while TFIIIA and
734 TFIIIC are assembly factors. *Cell* **60**, 235–245 (1990).
- 735 43. Blair, R. H., Goodrich, J. A. & Kugel, J. F. Single-molecule fluorescence resonance
736 energy transfer shows uniformity in TATA binding protein-induced DNA bending
737 and heterogeneity in bending kinetics. *Biochemistry* **51**, 7444–7455;
738 10.1021/bi300491j (2012).
- 739 44. Gietl, A. *et al.* Eukaryotic and archaeal TBP and TFB/TF(II)B follow different
740 promoter DNA bending pathways. *Nucleic Acids Research* **42**, 6219–6231;
741 10.1093/nar/gku273 (2014).
- 742 45. Schluesche, P. *et al.* Dynamics of TBP binding to the TATA box. *16057422* **6862**,
743 68620E - 68620E - 8; 10.1117/12.769177 (2008).
- 744 46. Heiss, G. *et al.* Conformational changes and catalytic inefficiency associated with
745 Mot1-mediated TBP-DNA dissociation. *Nucleic Acids Research* **47**, 2793–2806;
746 10.1093/nar/gky1322 (2019).
- 747 47. Zarrabi, N., Schluesche, P., Meisterernst, M., Börsch, M. & Lamb, D. C. Analyzing the
748 Dynamics of Single TBP-DNA-NC2 Complexes Using Hidden Markov Models.
749 *Biophysical journal* **115**, 2310–2326; 10.1016/j.bpj.2018.11.015 (2018).
- 750 48. Delgadillo, R. F., Whittington, J. D. E., Parkhurst, L. K. & Parkhurst, L. J. The TATA-
751 binding protein core domain in solution variably bends TATA sequences via a three-
752 step binding mechanism. *Biochemistry* **48**, 1801–1809; 10.1021/bi8018724 (2009).
- 753 49. Masters, K. M., Parkhurst, K. M., Daugherty, M. A. & Parkhurst, L. J. Native human
754 TATA-binding protein simultaneously binds and bends promoter DNA without a
755 slow isomerization step or TFIIIB requirement. *Journal of Biological Chemistry* **278**,
756 31685–31690; 10.1074/jbc.M305201200 (2003).
- 757 50. Parkhurst, K. M., Richards, R. M., Brenowitz, M. & Parkhurst, L. J. Intermediate
758 species possessing bent DNA are present along the pathway to formation of a final
759 TBP-TATA complex 1 1Edited by R. Ebright. *Journal of Molecular Biology* **289**, 1327–
760 1341; 10.1006/jmbi.1999.2835 (1999).

- 761 51. Whittington, J. D. E. *et al.* TATA-binding protein recognition and bending of a
762 consensus promoter are protein species dependent. *Biochemistry* **47**, 7264–7273;
763 10.1021/bi800139w (2008).
- 764 52. Gouge, J. *et al.* Molecular mechanisms of Bdp1 in TFIIIB assembly and RNA
765 polymerase III transcription initiation. *Nature Communications* **8**, 130;
766 10.1038/s41467-017-00126-1 (2017).
- 767 53. Tyagi, M., Imam, N., Verma, K. & Patel, A. K. Chromatin remodelers: We are the
768 drivers!! *Nucleus (Austin, Tex.)* **7**, 388–404; 10.1080/19491034.2016.1211217
769 (2016).
- 770 54. Struhl, K. & Segal, E. Determinants of nucleosome positioning. *Nature Structural &*
771 *Molecular Biology* **20**, 267–273; 10.1038/nsmb.2506 (2013).
- 772 55. Funke, J. J. *et al.* Uncovering the forces between nucleosomes using DNA origami.
773 *Science advances* **2**, e1600974; 10.1126/sciadv.1600974 (2016).
- 774 56. Yan, J. & Marko, J. F. Effects of DNA-distorting proteins on DNA elastic response.
775 *Physical review. E, Statistical, nonlinear, and soft matter physics* **68**, 11905;
776 10.1103/PhysRevE.68.011905 (2003).
- 777 57. Nickels, P. C. *et al.* Molecular force spectroscopy with a DNA origami-based
778 nanoscopic force clamp. *Science (New York, N.Y.)* **354**, 305–307;
779 10.1126/science.aah5974 (2016).
- 780 58. Smith, S. B., Cui, Y. & Bustamante, C. Overstretching B-DNA: the elastic response of
781 individual double-stranded and single-stranded DNA molecules. *Science* **271**, 795–
782 799 (1996).
- 783 59. Kouzine, F., Levens, D. & Baranello, L. DNA topology and transcription. *Nucleus*
784 *(Austin, Tex.)* **5**, 195–202; 10.4161/nucl.28909 (2014).
- 785 60. Gietl, A. & Grohmann, D. Modern biophysical approaches probe transcription-
786 factor-induced DNA bending and looping. *Biochemical Society Transactions* **41**,
787 368–373; 10.1042/BST20120301 (2013).
- 788 61. Chien, F.-T. & van der Heijden, T. Characterization of nucleosome unwrapping
789 within chromatin fibers using magnetic tweezers. *Biophysical journal* **107**, 373–383;
790 10.1016/j.bpj.2014.05.036 (2014).

- 791 62. Kruithof, M. *et al.* Single-molecule force spectroscopy reveals a highly compliant
792 helical folding for the 30-nm chromatin fiber. *Nature Structural & Molecular Biology*
793 **16**, 534–540; 10.1038/nsmb.1590 (2009).
- 794 63. Cui, Y. & Bustamante, C. Pulling a single chromatin fiber reveals the forces that
795 maintain its higher-order structure. *Proceedings of the National Academy of*
796 *Sciences of the United States of America* **97**, 127–132; 10.1073/pnas.97.1.127
797 (2000).
- 798 64. Meng, H., Andresen, K. & van Noort, J. Quantitative analysis of single-molecule force
799 spectroscopy on folded chromatin fibers. *Nucleic Acids Research* **43**, 3578–3590;
800 10.1093/nar/gkv215 (2015).
- 801 65. Dieci, G. & Sentenac, A. Facilitated recycling pathway for RNA polymerase III. *Cell*
802 **84**, 245–252 (1996).
- 803 66. Dieci, G., Bosio, M. C., Fermi, B. & Ferrari, R. Transcription reinitiation by RNA
804 polymerase III. *Biochimica et biophysica acta* **1829**, 331–341;
805 10.1016/j.bbagr.2012.10.009 (2013).
- 806 67. Dieci, G. & Sentenac, A. Detours and shortcuts to transcription reinitiation. *Trends*
807 *in Biochemical Sciences* **28**, 202–209; 10.1016/S0968-0004(03)00054-9 (2003).
- 808 68. Han, Y., Yan, C., Fishbain, S., Ivanov, I. & He, Y. Structural visualization of RNA
809 polymerase III transcription machineries. *Cell Discovery* **4**, 40; 10.1038/s41421-018-
810 0044-z (2018).
- 811 69. Helbo, A. S., Lay, F. D., Jones, P. A., Liang, G. & Grønbaek, K. Nucleosome Positioning
812 and NDR Structure at RNA Polymerase III Promoters. *Scientific Reports* **7**, 41947;
813 10.1038/srep41947.
- 814 70. Schones, D. E. *et al.* Dynamic regulation of nucleosome positioning in the human
815 genome. *Cell* **132**, 887–898; 10.1016/j.cell.2008.02.022 (2008).
- 816 71. Zhang, Y. *et al.* Intrinsic histone-DNA interactions are not the major determinant of
817 nucleosome positions in vivo. *Nature Structural & Molecular Biology* **16**, 847–852;
818 10.1038/nsmb.1636 (2009).
- 819 72. Radman-Livaja, M. & Rando, O. J. Nucleosome positioning: how is it established, and
820 why does it matter? *Developmental biology* **339**, 258–266;
821 10.1016/j.ydbio.2009.06.012 (2010).

- 822 73. Sambrook, J. *Molecular cloning*. 3rd ed. (Cold Spring Harbor Laboratory Press, Cold
823 Spring Harbor, NY, 2001).
- 824 74. Douglas, S. M., Chou, J. J. & Shih, W. M. DNA-nanotube-induced alignment of
825 membrane proteins for NMR structure determination. *Proceedings of the National*
826 *Academy of Sciences of the United States of America* **104**, 6644–6648;
827 10.1073/pnas.0700930104 (2007).
- 828 75. Kapanidis, A. N. *et al.* Alternating-laser excitation of single molecules. *Accounts of*
829 *chemical research* **38**, 523–533; 10.1021/ar0401348 (2005).
- 830 76. Preus, S., Noer, S. L., Hildebrandt, L. L., Gudnason, D. & Birkedal, V. iSMS: single-
831 molecule FRET microscopy software. *Nature Methods* **12**, 593;
832 10.1038/nmeth.3435 (2015).
- 833 77. Bronson, J. E., Fei, J., Hofman, J. M., Gonzalez, R. L. & Wiggins, C. H. Learning rates
834 and states from biophysical time series: a Bayesian approach to model selection
835 and single-molecule FRET data. *Biophysical journal* **97**, 3196–3205;
836 10.1016/j.bpj.2009.09.031 (2009).
- 837 78. Schrimpf, W., Barth, A., Hendrix, J. & Lamb, D. C. PAM: A Framework for Integrated
838 Analysis of Imaging, Single-Molecule, and Ensemble Fluorescence Data. *Biophysical*
839 *journal* **114**, 1518–1528; 10.1016/j.bpj.2018.02.035 (2018).
- 840 79. Hellenkamp, B. *et al.* Precision and accuracy of single-molecule FRET
841 measurements-a multi-laboratory benchmark study. *Nature Methods* **15**, 669–676;
842 10.1038/s41592-018-0085-0 (2018).